# *The Journal of* Immunology

RESEARCH ARTICLE | MARCH 01 2012

# Glutathione Reductase Facilitates Host Defense by Sustaining Phagocytic Oxidative Burst and Promoting the Development of Neutrophil Extracellular Traps ⊘

Jing Yan; ... et. al

---

### Related Content

Glutathione reductase facilitates host defense by sustaining phagocytic oxidative burst and promoting the development of neutrophil extracellular traps (172.3)

*J Immunol* (May,2012)

The Phagocytosis-Associated Respiratory Burst in Human Monocytes Is Associated with Increased Uptake of Glutathione

*J Immunol* (September,2000)

The Role of Glutathione Reductase in Neutrophil Respiratory Burst and ERK Signaling

*J Immunol* (May,2016)

---

# Glutathione Reductase Facilitates Host Defense by Sustaining Phagocytic Oxidative Burst and Promoting the Development of Neutrophil Extracellular Traps

Jing Yan,*,† Xiaomei Meng,* Lyn M. Wancket,‡ Katherine Lintner,* Leif D. Nelin,* Bernadette Chen,* Kevin P. Francis,§ Charles V. Smith,¶ Lynette K. Rogers,* and Yusen Liu*,‡

**Glutathione reductase (Gsr) catalyzes the reduction of glutathione disulfide to glutathione, which plays an important role in the bactericidal function of phagocytes. Because Gsr has been implicated in the oxidative burst in human neutrophils and is abundantly expressed in the lymphoid system, we hypothesized that Gsr-deficient mice would exhibit marked defects during the immune response against bacterial challenge. We report in this study that Gsr-null mice exhibited enhanced susceptibility to *Escherichia coli* challenge, indicated by dramatically increased bacterial burden, cytokine storm, striking histological abnormalities, and substantially elevated mortality. Additionally, Gsr-null mice exhibited elevated sensitivity to *Staphylococcus aureus*. Examination of the bactericidal functions of the neutrophils from Gsr-deficient mice in vitro revealed impaired phagocytosis and defective bacterial killing activities. Although Gsr catalyzes the regeneration of glutathione, a major cellular antioxidant, Gsr-deficient neutrophils paradoxically produced far less reactive oxygen species upon activation both ex vivo and in vivo. Unlike wild-type neutrophils that exhibited a sustained oxidative burst upon stimulation with phorbol ester and fMLP, Gsr-deficient neutrophils displayed a very transient oxidative burst that abruptly ceased shortly after stimulation. Likewise, Gsr-deficient neutrophils also exhibited an attenuated oxidative burst upon encountering *E. coli*. Biochemical analysis revealed that the hexose monophosphate shunt was compromised in Gsr-deficient neutrophils. Moreover, Gsr-deficient neutrophils displayed a marked impairment in the formation of neutrophil extracellular traps, a bactericidal mechanism that operates after neutrophil death. Thus, Gsr-mediated redox regulation is crucial for bacterial clearance during host defense against massive bacterial challenge.** *The Journal of Immunology,* 2012, 188: 2316–2327.

T he oxidative burst plays an important role in the bactericidal action of phagocytes (1). Reactive oxygen species (ROS) produced during the oxidative burst by the phagocyte NADPH oxidase complex are not only required for pathogen clearance but also implicated in organ damage during sepsis (1–3). The phagosomal oxidative burst is initiated by a stimulus-dependent assembly of the NADPH oxidase complex after phagocytosis of bacterial pathogens (4, 5). A variety of signaling pathways have been shown to mediate NADPH oxidase activation, including PI3K (6–8), small GTPase Rac (9, 10), and protein kinases AKT and protein kinase Cδ (11–14). NADPH oxidase reduces molecular oxygen to yield $O_2^{\bullet-}$, which dismutes to produce $H_2O_2$. Myeloperoxidase (MPO) released from azurophilic granules catalyzes the conversion of $H_2O_2$ and $Cl^-$ to the highly bactericidal hypochlorous acid in the phagolysosomes. Defects in the subunits of NADPH oxidase resulting in diminished phagocytic oxidative burst are associated with chronic granulomatous disease (CGD), illustrating the critical role of the oxidative burst in host defense (15). In addition to mediating the direct bactericidal activity within phagolysosomes, ROS production in neutrophils is also crucial for the development of neutrophil extracellular traps (NETs) (16–18). NETs are a dense network of extracellular fibers primarily composed of neutrophilic chromatins and antimicrobial peptides (19). NET formation after neutrophil death, often referred to as NETosis, is a fascinating antimicrobial host defense mechanism, because NETs can capture and kill infecting microbes extracellularly (20–22).

Glutathione is critical for the elimination of $H_2O_2$ in the cytosol (23, 24). $H_2O_2$ is produced in the phagolysosomes near the membrane, and it can easily diffuse into the cytosol. In the cytosol, glutathione reacts with $H_2O_2$ through a chemical reaction catalyzed by glutathione peroxidase, resulting in glutathione disulfide (GSSG) (23, 24). Glutathione reductase (Gsr) catalyzes the regeneration of glutathione from GSSG (GSSG + NADPH + $H^+ \rightarrow$ 2GSH + $NADP^+$), utilizing NADPH generated by the hexose monophosphate shunt (HMPS). Therefore, Gsr perpetuates the GSH/GSSG cycle to facilitate the transfer of electrons from glucose to $H_2O_2$ to eliminate $H_2O_2$ within the cytosol, thus preventing oxidative damage to the phagocytes (23, 25). Although earlier

*Center for Perinatal Research, The Research Institute at Nationwide Children's Hospital, Department of Pediatrics, The Ohio State University College of Medicine, Columbus, OH 43205; †State Key Laboratory of Biocontrol, School of Life Sciences, Sun Yat-sen University, Guangzhou 510275, People's Republic of China; ‡Department of Veterinary Bioscience, The Ohio State University College of Veterinary Medicine, Columbus, OH 43221; §Caliper Life Sciences, Alameda, CA 94501; and ¶Center for Developmental Therapeutics, Seattle Children's Research Institute, Seattle, WA 98101

Abbreviations used in this article: BCNU, 1,3-bis(2-chloroethyl)-1-nitrosourea; b.w., body weight; CGD, chronic granulomatous disease; DHR123, dihydrorhodamine 123; Gsr, glutathione reductase; GSSG, glutathione disulfide; HMPS, hexose monophosphate shunt; MFI, mean fluorescence intensity; MPO, myeloperoxidase; NET, neutrophil extracellular trap; PI, propidium iodide; ROS, reactive oxygen species.

studies implicated Gsr in the regulation of phagocytic oxidative burst (24, 26, 27), the functional importance of Gsr in the immune response against bacterial infection in vivo has not been thoroughly investigated. Humans with only marginal GSR activity were reported in a family >30 y ago, and a compromised oxidative burst was observed in leukocytes from these individuals (26, 27). Gsr-deficient mice have been generated by chemical mutagenesis, and no obvious phenotype has been reported in these animals (28). To define the immune functions of Gsr, we backcrossed the Gsr-deficient mice to a C3H/HeN background and investigated the effects of Gsr deficiency on host defense against *Escherichia coli* and *Staphylococcus aureus* challenge. Our studies indicate that Gsr is essential for effective host defense against massive bacterial challenge by supporting phagocytosis, sustaining the oxidative burst, and facilitating the development of NETs.

## Materials and Methods

### Mice

Wild-type C3H/HeN mice (6–10 wk old) were purchased from Harlan Laboratories. The Gsr-deficient mice were originally generated in Dr. Walter Pretsch's laboratory by isopropyl methanesulfonate-induced random mutagenesis (28), and they had been backcrossed to the inbred C3H/E1 wild-type strain for at least 15 generations prior to shipping to our laboratory. The genetic mutation in these mice was characterized later as a 13-kb deletion that starts in intron 1 and ends in intron 5 of the *Gsr* gene (29). This deletion causes a frame shift in the resulting mutant Gsr mRNA, preventing its translation into a functional protein. The Gsr mutant mice obtained from Dr. Walter Pretsch were further crossbred to C3H/HeN mice for 10 generations in our laboratory and bred to homozygosity. Animals were kept with free access to food and water in a specific pathogen-free vivarium at 25°C with humidity between 30 and 70% and with a 12 h alternating light/dark cycle. Animals were treated humanely according to the National Institutes of Health guidelines, and all animal experiments were approved by the Institutional Animal Care and Use Committee of The Research Institute at Nationwide Children's Hospital.

### Abs, fluorophores, enzymes, and chemicals

For flow cytometry, the following Abs or fluorophores were used. F4/80-PE-Cy7 (BM8) and CD11b-eFluor 605NC (M1170) were purchased from eBioscience. Ly-6G-Pacific Blue (1A8) and Gr-1-Pacific Blue (RB6-8C5) were purchased from BioLegend. Dihydrorhodamine 123 (DHR123) was purchased from Invitrogen.

In the immunofluorescence experiments, the goat anti-mouse histone H2A.X (M-20) (sc-54607) and the rabbit anti-mouse neutrophil elastase (ab68672) were purchased from Santa Cruz Biotechnology and Abcam, respectively. Alexa Fluor 488 donkey anti-rabbit IgG (H+L) (A21206) and Alexa Fluor 546 donkey anti-goat IgG (H+L) (A11056) were purchased from Invitrogen and used as second Abs to detect neutrophil elastase and histone H2A, respectively. The DNA dyes Sytox Green and Hoechst 33342 were purchased from Invitrogen.

HRP and superoxide dismutase (SOD) were purchased from EMD Biosciences. Catalase was purchased from Worthington Biochemical. Luminol, isoluminol, 1,3-bis(2-chloroethyl)-1-nitrosourea (BCNU), PMA, and fMLP used in the oxidative burst experiments were purchased from Sigma-Aldrich.

### Sepsis, hematology analysis, and organ pathology

In the bacterial sepsis model, mice were infected either i.p. or i.v. with *E. coli* (O55:B5, ATCC 12014). To quantify the susceptibility of the two strains of mice to *E. coli* challenge, mice were infected with different doses of *E. coli*, and survival of these mice was monitored during 7 d. The $LD_{50}$ values were calculated with the PROBIT procedure using ASA9.2 software (SAS Institute). To perform hematological analyses and assess organ pathology, mice were euthanized 24 h after *E. coli* challenge to harvest blood and organs. Hematological analysis of blood was carried out using a Forcyte hematology analyzer (Oxford Science). To assess organ pathology, the tissue sections were stained with H&E and examined for histological abnormalities as previously described (30). TUNEL assays were performed to assess splenocyte apoptosis using an In Situ Cell Death Detection Kit from Roche Applied Sciences, according to the manufacturer's recommendations.

To assess the sensitivity of wild-type and Gsr-null mice to *S. aureus*, we infected mice i.v. with *S. aureus* (FDA 209P, ATCC 6538P) at a dose of $4 \times 10^8$ CFU per animal. Animal survival was monitored during 5 d.

### Bacterial burden

Bacterial burden in the blood and spleens was quantified by bacterial culture, as previously described (31, 32).

To monitor bacterial burden in vivo in live animals, mice were infected with *E. coli* Xen-14 (Caliper Life Sciences), which is a bioluminescent derivative of an enteropathogenic strain of *E. coli* (WS2572). *E. coli* Xen-14 was generated by stable integration of the *Photorhabdus luminescens luxCDABE* operon into the bacterial chromosome (33, 34). *E. coli* Xen-14 cells in live animals were monitored using a Xenogen IVIS Spectrum imaging system (Caliper Life Sciences).

### Phagocytosis and in vitro bacterial killing assays

The phagocytic activity of wild-type and Gsr-null phagocytes was assessed using bone marrow neutrophils. Neutrophils were isolated from mouse bone marrow as previously described (35). Texas Red-conjugated or the pH-sensitive pHrodo-conjugated *E. coli* bioparticles (Invitrogen) were opsonized using serum according to the manufacturer's instructions. Neutrophils were incubated with fluorophore-conjugated *E. coli* bioparticles at 37°C or on ice (as a control) for 1 h. Cells were then stained with neutrophil markers CD11b and Ly6G, and phagocytosis of the *E. coli* particles by neutrophils (CD11b+Ly6G^high) was assessed by flow cytometry.

The bactericidal activity of wild-type and Gsr-deficient phagocytes was assessed in vitro using bone marrow neutrophils or whole blood. Serum preopsonized *E. coli* (O5:B55) was incubated with bone marrow neutrophils at 37°C for 15 min at a multiplicity of infection of 10. When whole blood was used, blood samples (100 μl) were incubated with $10^7$ CFU freshly cultured *E. coli* at 37°C for 15 min. Leukocytes were then lysed with 0.05% saponin, and viable bacteria in the lysates were counted after culture on Luria-Bertani agar plates.

### Ex vivo and in vivo oxidative burst

Phagocytic oxidative burst in blood leukocytes ex vivo was assessed by chemiluminescence imaging essentially as described by Gross et al. (36). Briefly, leukocytes were purified from 200 μl heparinized whole blood after lysing erythrocytes, incubated with 100 μM luminol, and then stimulated with either 5 μM PMA or vehicle (DMSO) in a black 96-well plate. The oxidative burst in leukocytes was assessed by taking sequential images in an IVIS Spectrum imaging system. To determine the production of intracellular ROS, HRP (4 U/ml), catalase (3000 U/ml), and superoxide dismutase (50 U/ml) were added to the reaction 10 min before PMA or fMLP stimulation (37). For detection of extracellular ROS, the oxidative burst assays were performed using isoluminol (100 μM) in the presence of HRP (4 U/ml) (37).

To assess the oxidative burst in vivo, mice were infected with *E. coli* (O55:B5) i.p. Each animal was given one dose of luminol (200 μg/g body weight [b.w.]) i.p. at a given time postinfection and immediately placed in an IVIS Spectrum imaging system to document the oxidative burst activity at that time. To assess phagocytic oxidative burst after *E. coli* stimulation ex vivo, 100 μl heparinized whole blood was incubated with *E. coli* (serotype O55:B5) for 15 min in the presence of DHR123, which can be oxidized to fluorescent rhodamine 123 by ROS. The leukocytes were then stained with Abs against different cell markers. Oxidative burst activity in neutrophils (CD11b+Gr-1^highF4/80^−) and monocytes (CD11b+Gr-1^lowF4/80^+) in the blood was analyzed by flow cytometry. The results were analyzed using FlowJo software (Tree Star).

### HMPS activity

$^{14}CO_2$ production from D-glucose-1-$^{14}C$ was determined as a measure of HMPS activity, essentially according to the procedures used by Pachman et al. (38). Neutrophils were isolated from mouse bone marrow (35). Bone marrow neutrophils were resuspended to a density of $3 \times 10^6$ cells/ml in HBSS containing 1 mg/ml glucose and added to Eppendorf tubes containing 1 μCi of D-glucose-1-$^{14}C$ (Perkin Elmer), which were suspended on strings in 40-ml glass vials with septum caps. The cells were stimulated with 5 μM PMA or same volume of vehicle (DMSO) at 37°C for 2 h. The released $^{14}CO_2$ was captured in 2 ml hyamine hydroxide (PerkinElmer) in the bottom of the glass vials. At the end of the incubation, the reaction was stopped by injecting 0.3 ml 0.2 M $H_2SO_4$ into the Eppendorf tubes through the septum, which also facilitates the release of $^{14}CO_2$ from the culture and the capture by hyamine hydroxide. Glass vials were left at 37°C overnight to capture $CO_2$. Hyamine was transferred to glass vials containing 5 ml scintillation liquid (Insta-Fluor Plus; PerkinElmer) and radioactivity was measured in a scintillation counter (Packard Instrument).

### Immunofluorescence assays and scanning electron microscopy

Neutrophils were purified from mouse bone marrow by Percoll gradient centrifugation (35) and seeded on glass coverslips in 24-well plates. After

60 min, cells were given medium containing vehicle (DMSO), PMA (100 nM), or *E. coli* (multiplicity of infection of 50) and cultured for an additional 16 h for the development of NETs. Cells on the coverslips were fixed and then subjected to DNA staining or immunofluorescence staining procedures, essentially as previously described (39, 40). Fluorescent images were acquired using a scanning confocal microscope (LSM-710; Zeiss) and analyzed using LSM 710 ZEN software. Z-series images were obtained at a step size of 0.5 μm over a range of 10 μm for each field. The images were compiled to construct the images. For quantification of NET formation, 10 random ×100 oil fields were examined by two observers in a blinded fashion to count the numbers of neutrophils that either formed NETs or preserved their lobulated nuclear structure.

To assess NET formation with the scanning electron microscope, bone marrow neutrophils treated with PMA or *E. coli* for 16 h were fixed with 4% paraformaldehyde overnight and then incubated with 2.5% glutaraldehyde for 30 min. The fixed cells were then treated with 1% osmium tetroxide solution and 1% tannic acid, dehydrated using a graded series of ethanol, and dried in hexamethyldisilizane, essentially as previously described (41). The specimens were subsequently mounted on stubs and sputter-coated with gold. Finally, the specimens were visualized using an S-4800 scanning electron microscope (Hitachi).

*Western blotting and ELISA*

Western blot analysis and ELISA were performed essentially as previously described (31, 42).

*Statistical analyses*

Differences in survival between wild-type and Gsr-deficient mice after bacterial challenge were determined by Kaplan–Meier analysis. Differences in other biological parameters between the wild-type and Gsr-deficient groups were analyzed using a Wilcoxon signed rank test (when $n < 10$) or Student $t$ test (when $n \geq 10$), or by two-way ANOVA (when time was also a variable). When the data were not normally distributed, the values were log-transformed prior to statistical analysis. A $p$ value of $<0.05$ was considered significant.

## Results

*Gsr-deficient mice exhibit impaired bactericidal activity and increased mortality following* E. coli *and* S. aureus *infection*

Gsr was detected as a 54-kDa protein in bone marrow, spleen, thymus, brain, lung, liver, kidney, and eyes in wild-type mice. As expected, Gsr protein was not detected in Gsr-null mice (data not shown). The Gsr-null mice are fertile and indistinguishable from wild-type mice in the absence of challenge. Comprehensive phenotypic analyses in the Phenotyping Core Facility of The Ohio State University College of Veterinary Medicine did not reveal any abnormalities in blood chemistry or organ histology (data not shown). Hematological analysis of the blood of Gsr-null mice did not reveal any obvious abnormalities in erythrocyte, leukocyte, or platelet counts (Table I). Histological evaluation of bone marrow from Gsr-null mice revealed appropriate cellularity with a normal myeloid-to-erythroid ratio and orderly maturation (data not shown). Lymphoid tissues also appeared normal (data not shown). These results collectively indicate that Gsr is not essential for survival of mice in a vivarium setting.

Although previous studies of the neutrophils from human subjects with marginal GSR activity have implicated this enzyme in phagocytic oxidative burst (26, 27), the functional importance of Gsr in host defense against bacteria in vivo has not been firmly established. To assess the functional importance of Gsr in host defense against bacterial challenge, we investigated the effects of Gsr deficiency on animal survival in a Gram-negative bacterial sepsis model. Wild-type and Gsr-null mice were infected i.p. or i.v. with *E. coli* (serotype O55:B5), and animal survival was monitored during 7 d (Fig. 1A). Remarkably, administration of *E. coli* i.p. at a dose of $8.3 \times 10^6$ CFU/g b.w. killed all Gsr-null mice within 48 h, whereas infection with the same dose of *E. coli* did not result in death in any of the wild-type mice (Fig. 1A, *left panel*). Similarly, *E. coli* infection i.v. at a dose of $2.5 \times 10^7$ CFU/g b.w. resulted in 70% mortality in Gsr-null mice, whereas the identical dose of *E. coli* did not cause any death in wild-type mice (Fig. 1A, *right panel*). Kaplan–Meier analysis revealed a significant difference in survival between the two groups.

To quantify the effects of Gsr deficiency on the animal susceptibility to *E. coli* challenge, we infected wild-type and Gsr-deficient mice with different doses of *E. coli* (O5:B55) and assessed animal survival during 7 d (Table II). The LD$_{50}$ values of wild-type and Gsr-deficient mice upon *E. coli* infection were estimated to be $1.5 \times 10^7$ and $4.0 \times 10^6$ CFU/g b.w., respectively. Our results indicate that Gsr deficiency renders mice substantially more susceptible to *E. coli* challenge.

To understand the underlying cause of the increased mortality in *E. coli*-infected Gsr-null mice, bacterial loads in the blood and spleens were assessed by colony formation assays. The median bacterial burdens in the blood and spleens of *E. coli*-infected Gsr-null mice were 10- to 100-fold higher than in similarly infected wild-type mice (Fig. 1B). The bactericidal defect of Gsr-null mice was further confirmed by assessing bacterial burden using noninvasive optical imaging in vivo. Mice were first infected with a bioluminescent pathogenic *E. coli* strain, Xen-14 (33, 34), and the bioluminescent bacteria in the infected mice were subsequently monitored using a Xenogen IVIS Spectrum imaging system (Fig. 1C). Hematological analyses of the *E. coli*-infected mice indicated that the defect of Gsr-deficient mice in bacterial clearance was not due to failure of leukocytes to emigrate into the circulation, because leukocyte counts in *E. coli*-infected wild-type and Gsr-deficient mice were comparable (Table I).

To assess whether Gsr deficiency also compromises host defense against *S. aureus*, the most common cause of infection in CGD patients (43), we challenged wild-type and Gsr-deficient mice with *S. aureus* i.v. and assessed animal survival and bacterial burden (Fig. 2). Gsr deficiency significantly decreased animal survival following *S. aureus* infection (Fig. 2A). Compared to wild-type mice, Gsr-null mice exhibited greater bacterial burden in both blood and the spleens (Fig. 2B).

*Cytokine storm and histological abnormalities in Gsr-deficient mice after* E. coli *challenge*

Histological analyses revealed remarkable differences in the livers and spleens between *E. coli*-infected wild-type and Gsr-null mice 24 h after infection (Fig. 3), whereas histological differences were

Table I.  Blood hematological analysis in wild-type and Gsr-null mice

| | Neutrophil Count (%) | Monocyte Count (%) | Eosinophil Count (%) | Lymphocyte Count (%) | RBC Count (×10⁶) | Platelet Count (×10³) |
|---|---|---|---|---|---|---|
| Wild-type | 1900 ± 589 (52 ± 6.4) | 127 ± 7 (4.3 ± 1.0) | 23 ± 19 (0.7 ± 0.5) | 1343 ± 191 (42 ± 5.5) | 7.4 ± 0.5 | 845 ± 189 |
| Gsr-null | 1000 ± 104 (37 ± 2.4) | 233 ± 28 (8.5 ± 1.0) | 6.7 ± 3.3 (0.2 ± 0.0) | 1500 ± 31 (55 ± 2.4) | 7.6 ± 0.3 | 742 ± 80 |
| Wild-type, *E. coli* | 900 ± 277 (63 ± 7.8) | 33 ± 24 (3.3 ± 2.4) | 60 ± 21 (4.5 ± 1.7) | 347 ± 19 (26 ± 4.2) | 8.4 ± 0.2 | 358 ± 17 |
| Gsr-null, *E. coli* | 3600 ± 1507 (85 ± 5.5) | 130 ± 26 (4.9 ± 2.4) | 83 ± 36 (1.7 ± 0.5) | 213 ± 23 (8.1 ± 3.6) | 7.4 ± 0.7 | 437 ± 73 |

Blood was harvested from either uninfected or *E. coli* (O5:B55)-infected mice ($8.3 \times 10^6$ CFU/g b.w., i.p.) 24 h after infection. Hematological analysis was carried out to assess the counts of each blood population using a Forcyte hematology analyzer (Oxford Science). Count values are given as counts per microliter. Number in parenthesis represents the percentage that a given cell type constitutes in the leukocyte population. The values are presented as mean ± SEM ($n = 3$).

**FIGURE 1.** Gsr-deficient mice exhibit impaired bactericidal activity and increased susceptibility to *E. coli* challenge. (**A**) Survival curves of wild-type and Gsr-null mice after *E. coli* challenge. *E. coli* (O55:B5) was introduced either i.p. (*left panel*) or i.v. (*right panel*). For i.p. infection, mice (*n* = 12 for wild-type; *n* = 11 for Gsr-null) were challenged with *E. coli* at a dose of 8.3 $\times 10^6$ CFU/g b.w. For i.v. infection, mice (*n* = 15 for both strains) were challenged with *E. coli* at a dose of 2.5 $\times 10^7$ CFU/g b.w. (**B**) Bacterial burden in the blood and spleens after *E. coli* challenge. Mice were infected i.v. with *E. coli* (O55:B5) at a dose of 2.5 $\times 10^7$ CFU/g b.w. and euthanized 24 h later. Blood and spleens were excised aseptically. Blood and spleen homogenates were cultured on Luria-Bertani agar plates. Colony numbers were normalized to blood volume or spleen weight. Bars represent the median values. *$p < 0.05$, comparing between genotypes (Wilcoxon signed rank test). (**C**) Bacterial load detected by in vivo bioluminescent imaging. Mice were infected i.p. with bioluminescent *E. coli* Xen-14 cells (8.3 $\times 10^6$ CFU/g b.w.). After 24 h, bioluminescent *E. coli* was visualized using an IVIS Spectrum imaging system (exposure time, 1 min; field of view, D; binning, 8). Results shown are representative images from three experiments.
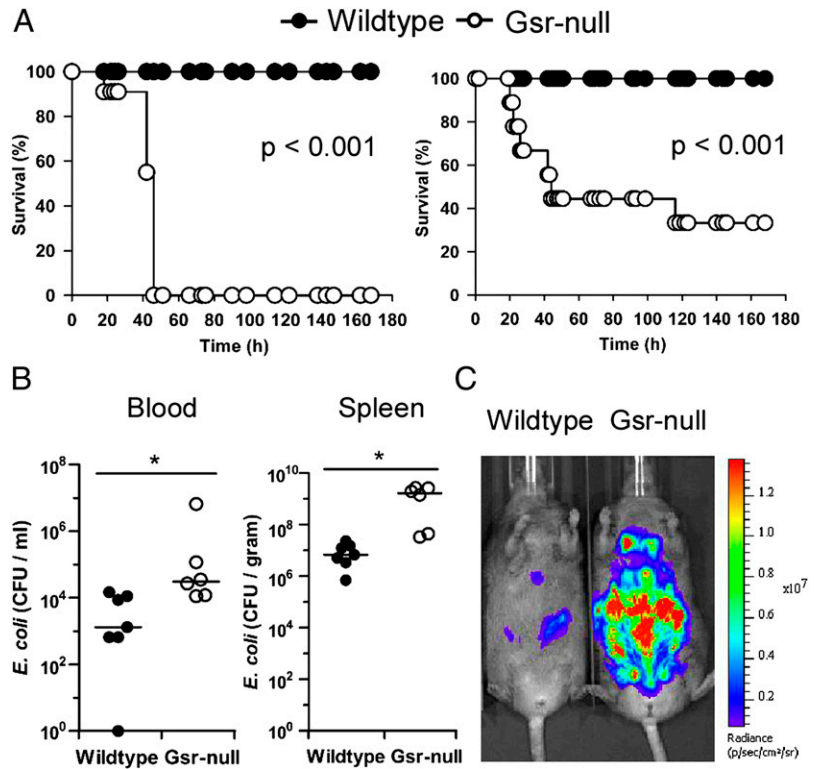
not observed in the lungs, hearts, or kidneys (data not shown). In Gsr-null mice, *E. coli* infection resulted in many medium and large necrotic foci with numerous infiltrating polymorphonuclear cells in the livers (Fig. 3A). However, in wild-type mice, hepatic necrotic foci were rare and tiny when present. Major histological differences were also observed in the spleens between *E. coli*-infected wild-type and Gsr-deficient mice (Fig. 3B). Although the boundaries between white and red pulps were blurred in the spleens of *E. coli*-infected wild-type mice (Fig. 3B, *upper middle panel*), the boundaries between white and red pulps remained clearly defined in Gsr-deficient mice (Fig. 3B, *lower middle panel*). Additionally, *E. coli* infection resulted in massive lymphocyte apoptosis in the white pulp regions of the wild-type spleens, as indicated by H&E staining (Fig. 3B, *upper right panel*) and TUNEL assays (Fig. 3C). In contrast, little evidence of apoptosis was seen in the white pulp of the spleens from *E. coli*-infected Gsr-null mice (Fig. 3B, *lower right panel*, 3C). However, greater numbers of neutrophils in the red pulp regions of the spleens were observed in *E. coli*-infected Gsr-null mice than in similarly infected wild-type mice (Fig. 3B, *left column*).

Because excessive production of a variety of proinflammatory cytokines plays an important role in the pathophysiology of septic shock and mortality after bacterial infection (44), we assessed serum cytokine and chemokine levels in *E. coli*-infected mice. Shortly after *E. coli* administration (1–3 h), no obvious differences

between wild-type and Gsr-null mice were observed in serum levels of several prominent cytokines (TNF-α, IL-6, and IL-10) and chemokines (KC, MCP-1, and MIP-1α) (Fig. 4). By 6 h, serum cytokine and chemokine levels tended to be higher in Gsr-null mice than in wild-type mice. At 24 h, the levels of TNF-α, IL-6, and MIP-1α had declined substantially in wild-type mice. In contrast, the levels of all six cytokines and chemokines either remained elevated or increased further in Gsr-deficient mice, indicating cytokine storms in these animals. These results suggest that unlike the short-lived acute inflammatory response in wild-type mice, the inflammatory response in Gsr-null mice was sustained or enhanced, perhaps due to the tremendous bacterial burdens in these animals.
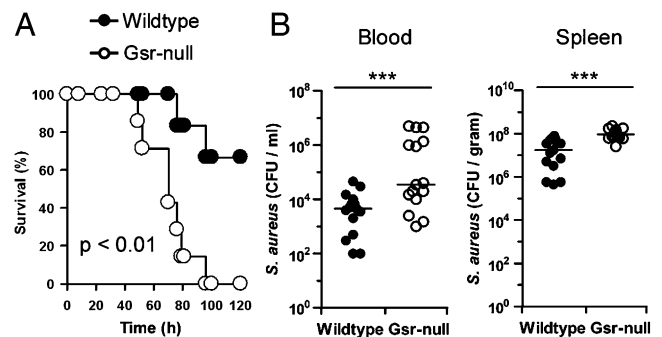
**Table II.** Survival of mice after i.p. *E. coli* infection

| Dose of Infection (CFU/g b.w.) | Survived[a]/Total | |
| --- | --- | --- |
| | Wild-Type | Gsr-Null |
| 9.3 $\times 10^5$ | 5/5 | 5/5 |
| 2.8 $\times 10^6$ | 5/5 | 5/5 |
| 8.3 $\times 10^6$ | 12/12 | 0/11 |
| 2.5 $\times 10^7$ | 1/5 | 0/5 |

[a]Number represents animals that survived after 7 d.



**FIGURE 2.** Gsr-deficient mice display increased mortality and elevated bacterial burden after *S. aureus* infection. (**A**) Survival curves for wild-type and Gsr-null mice after *S. aureus* challenge. *S. aureus* (FDA 209P) was introduced i.v. at a dose of 4.0 $\times 10^8$ CFU/mouse. Survival of mice (*n* = 6 for wild-type; *n* = 7 for Gsr-null) was monitored for 5 d. (**B**) Bacterial burden in the blood and spleens after *S. aureus* challenge. Mice were infected i.v. with *S. aureus* (FDA 209P) at a dose of 2.0 $\times 10^8$ CFU/animal and euthanized 24 h later. Blood and spleens were harvested aseptically, and bacterial load was assessed by culture on tryptic soy broth agar plates. Bars represent the median values. ***$p < 0.001$, comparing between genotypes (Student *t* test).
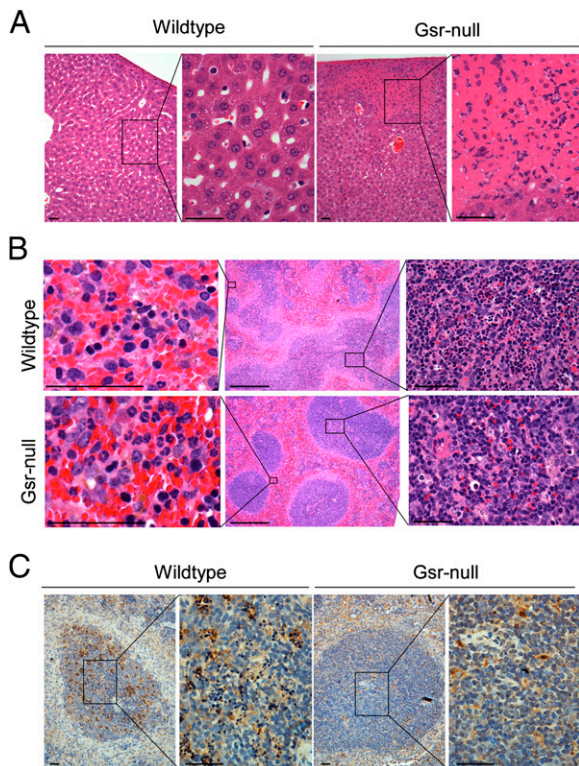
**FIGURE 3.** Histological images of the livers and spleens of *E. coli*-infected wild-type and Gsr-deficient mice. Mice were challenged i.p. with *E. coli* (O55:B5) at a dose of 8.3 $\times 10^6$ CFU/g b.w. and euthanized 24 h later. The livers and spleens were fixed, and tissue sections were stained with H&E or subjected to TUNEL assays. (**A**) Histology of the livers of *E. coli*-infected wild-type and Gsr-deficient mice prepared by H&E staining. Large number of neutrophils and dead hepatocytes are seen in the necrotic foci. (**B**) Histology of the spleens of *E. coli*-infected wild-type and Gsr-deficient mice prepared by H&E staining. Panels in the *center column* represent the low-magnification images of the spleens. Note the blurred boundaries between white and red pulp in the wild-type mice, whereas the boundaries between white and red pulp in the Gsr-deficient mice are well defined. Panels in the *left column* represent the high magnification of the red pulp regions. Note the markedly more abundant neutrophils in the Gsr-deficient mice. Panels in the *right column* represent the high magnification of the white pulp regions. Note the massive cell death in the white pulps of wild-type mice but not in the Gsr-deficient mice. (**C**) Apoptotic cells detected by TUNEL assays in the white pulps of the spleens. Paraffin-embedded spleen sections were subjected to TUNEL assays to detect apoptotic cells. The section was counterstained with hematoxylin. Apoptotic cells are stained brown in the spleen sections. Scale bars in (A)–(C) indicate 100 μm except in the center column of (B), where the bars indicate 1 mm. Results shown are representative images.

*Defects of Gsr-null phagocytes in phagocytosis and bactericidal function in vitro*

Because phagocytes play a critical role in host defense against extracellular bacteria (1) and Gsr-deficient mice displayed higher bacterial burden, we investigated the effects of Gsr deficiency on phagocytic activity. The phagocytic activity of bone marrow neutrophils in wild-type and Gsr-null mice was assessed by flow cytometry, using pH-sensitive pHrodo-conjugated *E. coli* bioparticles. Compared to wild-type neutrophils, Gsr-null neutrophils engulfed fewer *E. coli* particles, indicated by the leftward shift of the fluorescence spectrum (Fig. 5A, *upper row*) and decreased mean fluorescence intensity (MFI) in these cells (Fig. 5A, *upper row*, bar graph). To rule out the possibility that defects in phagocytosis in Gsr-null phagocytes might be caused by potential differences in the pH of phagosomes between the two groups, we

also assessed phagocytic properties of wild-type and Gsr-deficient neutrophils using Texas Red-conjugated *E. coli* particles. Similar phagocytic defects in Gsr-deficient neutrophils were also observed with Texas Red-conjugated *E. coli* particles (Fig. 5A, *lower row*). We also examined the phagocytic properties of wild-type and Gsr-deficient neutrophils used pHrodo-conjugated *S. aureus* and found that phagocytosis of *S. aureus* by the Gsr-deficient neutrophils was also compromised (data not shown).

To investigate whether Gsr-deficient phagocytes exhibit defects in bactericidal function in vitro, we incubated *E. coli* with bone marrow neutrophils or whole blood, lysed the leukocytes, and counted viable bacteria by culture on Luria-Bertani agar (Fig. 5B). Significantly more viable *E. coli* were detected after incubation with Gsr-deficient neutrophils than following incubation with wild-type neutrophils (Fig. 5B, *left graph*), indicating a bactericidal defect associated with Gsr deficiency. Likewise, more viable *E. coli* were also detected after incubation with blood samples from Gsr-null mice than after incubation with blood samples from wild-type mice (Fig. 5B, *right graph*).

*Gsr-deficient phagocytes exhibit impaired oxidative burst*

A major bactericidal mechanism used by phagocytes is the generation of ROS via the oxidative burst (1). We assessed the oxidative burst in wild-type and Gsr-null leukocytes. The oxidative burst in response to PMA in wild-type and Gsr-null blood leukocytes ex vivo was measured by chemiluminescence assays utilizing luminol and a Xenogen IVIS Spectrum imaging system (Fig. 6A). Upon PMA stimulation, wild-type leukocytes underwent a robust oxidative burst that lasted for >1 h (Fig. 6B). In contrast, Gsr-null leukocytes displayed only a very short oxidative burst, which abruptly ceased within 3 min. The total oxidative burst activity was substantially greater in wild-type than in Gsr-null leukocytes (Fig. 6C). We estimated that PMA-stimulated Gsr-deficient leukocytes exhibited an 80% decrease in ROS production relative to wild-type leukocytes. Because luminol-based chemiluminescence detection of the oxidative burst is dependent on MPO (36), which is expressed only in phagocytes (45), our results indicate that Gsr deficiency compromises the oxidative burst in phagocytes. Supporting the critical role of Gsr in the phagocytic oxidative burst, BCNU, a pharmacological inhibitor of Gsr (37), abolished the PMA-induced oxidative burst in phagocytes from the blood of wild-type mice (Fig. 6D).

Because luminol-based chemiluminescence detection of the oxidative burst is dependent on MPO (36), deficiency in oxidative burst in Gsr-deficient phagocytes might represent a defect in MPO activity in the Gsr-null phagocytes. In such a situation, addition of excessive HRP to the assay may minimize the difference in chemiluminescence between PMA-stimulated wild-type and Gsr-deficient phagocytes. Addition of HRP into the reactions enhanced the oxidative burst-dependent chemiluminescence (Fig. 6E). However, addition of HRP did not eliminate the differences in chemiluminescence between the phagocytes from the two genotypes (Fig. 6E, *left graph*), indicating that the difference in the oxidative burst between wild-type and Gsr-deficient phagocytes was not due to potential defects in MPO secretion in Gsr-null phagocytes. SOD catalyzes the dismutation of $O_2^{\bullet-}$ to $H_2O_2$, which in turn can be eliminated by catalase. Addition of both SOD and catalase into the reaction allows for the distinction between total and intracellular ROS (Fig. 6E, *middle graph*). Additionally, we assessed extracellular ROS release using isoluminol as a substrate, because isoluminol is more polar and hydrophilic and thus is less cell membrane permeable (Fig. 6E, *right graph*). These approaches indicate that Gsr-deficient phagocytes not only released less ROS intracellularly, but they also released less ROS to the

**■ Wildtype □ Gsr-null**



FIGURE 4. Gsr-deficient mice develop cytokine storm after *E. coli* challenge. Mice were challenged i.p. with *E. coli* (O55:B5) at a dose of $8.3 \times 10^6$ CFU/g b.w. and euthanized at the indicated time points. Blood was collected by cardiac puncture, and cytokines and chemokines in the serum were measured by ELISA. Data in the graphs represent means ± SEM of at least four independent experiments. $*p < 0.05$, $**p < 0.01$, $***p < 0.001$, comparing between genotypes (Wilcoxon signed rank test).
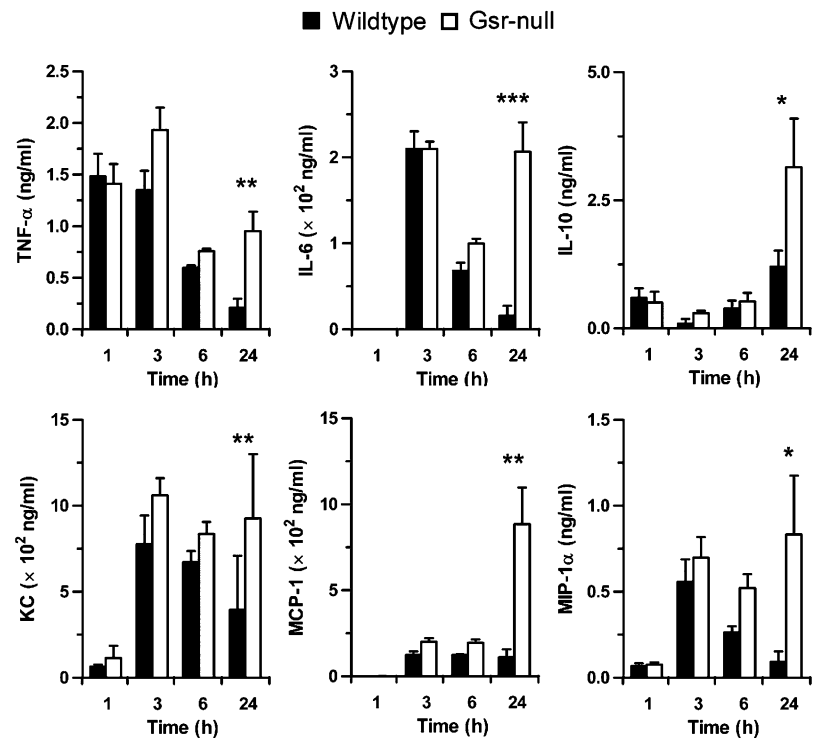
extracellular environment. Likewise, Gsr-deficient phagocytes exhibited a significant defect in the oxidative burst during the response to fMLP, an *N*-formylated peptide derived from bacterial proteins (data not shown).

The process of oxidative burst in phagocytes is coupled to anaerobic glycolysis through the HMPS (1). We assessed HMPS activity by determining the conversion of glucose-1-$^{14}$C to $^{14}$CO$_2$ in bone marrow neutrophils (Fig. 6F). The basal levels of glucose consumption were comparable between wild-type and Gsr-deficient neutrophils. PMA stimulation markedly enhanced $^{14}$CO$_2$ production in wild-type neutrophils. Compared to wild-type neutrophils, $^{14}$CO$_2$ production in Gsr-deficient neutrophils was significantly attenuated. Similar results were observed using whole blood from wild-type and Gsr-null mice (data not shown). It has been shown that PMA induces prompt neutrophil death, although not through the typical apoptosis or necrosis mechanisms (46). Because Gsr is involved in the regeneration of glutathione, a major cellular antioxidant, we assessed whether Gsr-deficient phagocytes exhibit altered cell viability upon induction of the oxidative burst by PMA (Fig. 6G). PMA stimulation of wild-type bone marrow neutrophils for 60 min induced a small increase in propidium iodide (PI)-positive (dead) cells, from 3 to 7%. In contrast, PMA stimulation of Gsr-deficient bone marrow neutrophils substantially increased the number of PI-positive cells (from 4 to 23%). PMA treatment did not significantly alter the viability of macrophages derived from either wild-type or Gsr-deficient bone marrow (data not shown). These results suggest that increased cell death as the result of Gsr deficiency contributes to the bactericidal defects of Gsr-null mice.

To examine the effects of Gsr deficiency on phagocytic oxidative burst ex vivo after *E. coli* infection, heparinized blood was incubated with *E. coli* (O55:B5) in the presence of DHR123, which becomes fluorescent rhodamine 123 after oxidation. Blood leukocytes were then stained with surface markers to quantify oxidative burst in neutrophils and monocytes by flow cytometry (Fig. 7A). *E. coli* induced a substantial oxidative burst in both wild-type neutrophils and monocytes in a dose-dependent manner, while the

oxidative burst in neutrophils was significantly stronger than that in monocytes. The oxidative burst was significantly weaker in Gsr-deficient neutrophils than in wild-type neutrophils (Fig. 7A, *upper panels*). Although 50% of wild-type neutrophils underwent oxidative burst after incubation with the highest dose of *E. coli*, only <20% of Gsr-deficient neutrophils underwent oxidative burst (Fig. 7A, *upper left panel*). Moreover, the MFI of the wild-type neutrophils was also significantly higher than that of the Gsr-null neutrophils (Fig. 7A, *upper right panel*), indicating that less ROS were produced on a per cell basis in Gsr-deficient neutrophils. The oxidative burst in *E. coli*-stimulated monocytes also tended to be higher in the wild-type group (Fig. 7A, *lower panels*).

The oxidative burst in vivo in *E. coli*-infected wild-type and Gsr-null mice was assessed by luminol chemiluminescence using a Xenogen IVIS Spectrum imaging system. Challenge of wild-type mice with *E. coli* resulted in an appreciable oxidative burst within 60 min, and the oxidative burst in these mice lasted for at least 6 h (Fig. 7B). The oxidative burst in *E. coli*-infected Gsr-null mice was substantially weaker than in the wild-type mice. Neither luminol administration alone nor *E. coli* infection alone (data not shown) resulted in detectable luminescence in either wild-type or Gsr-null mice. Taken together, these results indicate that the oxidative burst in Gsr-deficient phagocytes is impaired both ex vivo and in vivo, providing an explanation for the diminished bactericidal activity in Gsr-null mice.

*Gsr disruption compromises the development of NETs*

It has been shown that NET formation depends on the oxidative burst (17). Because Gsr-deficient neutrophils exhibited a substantial defect in the oxidative burst (Figs. 6, 7), we examined the effect of Gsr deficiency on NET formation following either PMA or *E. coli* stimulation. Unstimulated and PMA-stimulated bone marrow neutrophils were stained with Sytox Green to visualize DNA. Without stimulation, most neutrophils (~60%) from both wild-type and Gsr-null mice maintained a lobulated nuclear structure, whereas ~40% of the neutrophils exhibited a delobulated nuclear structure, as indicated by DNA staining (Fig. 8A). Upon
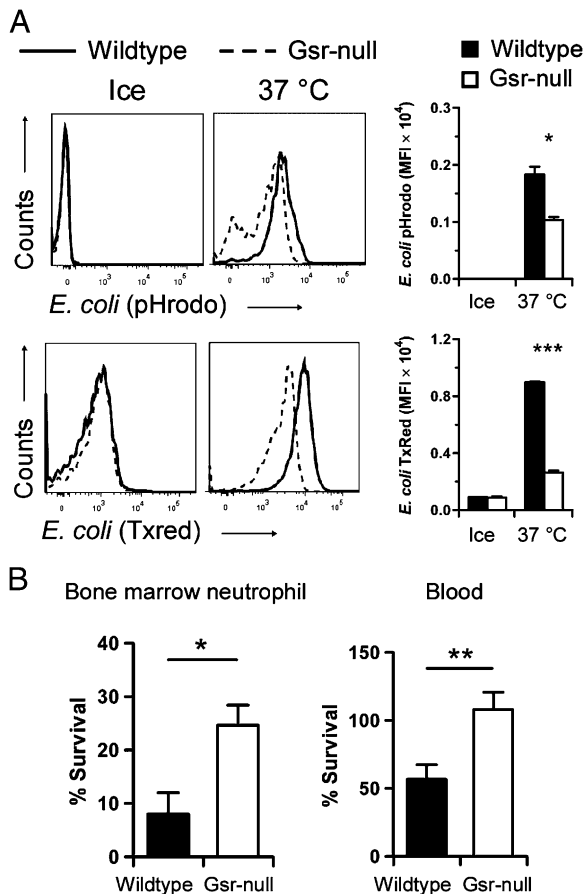
**FIGURE 5.** Compromised phagocytosis and ex vivo bacterial killing in Gsr-deficient neutrophils. (**A**) Impaired phagocytic function of Gsr-deficient neutrophils toward *E. coli*. Bone marrow neutrophils isolated from wild-type or Gsr-deficient mice were incubated with pHrodo-conjugated (*upper row*) or Texas Red (TxRed)-conjugated *E. coli* (*lower row*) bioparticles (200 μg/ml) on ice (control) or at 37°C for 1 h (*E. coli*) and then analyzed by flow cytometry. Representative histogram data are shown. Graphs on the *right* depict the MFI of *E. coli* particles engulfed by neutrophils. (**B**) Killing of *E. coli* (O55:B5) in vitro by wild-type and Gsr-deficient phagocytes. *Left graph,* Bone marrow neutrophils ($10^6$) were incubated with serum-opsonized *E. coli* ($10^7$ CFU) for 15 min at 37°C. As a control, the bacteria were also incubated with medium that contains no leukocytes. *Right graph,* Whole blood samples (100 μl) were incubated with *E. coli* ($10^7$ CFU) at 37°C for 15 min. As a control, the bacteria were incubated with 100 μl serum. After incubation, the leukocytes were lysed with saponin and the live bacteria were counted after culture on Luria-Bertani agar plates. Survival of bacteria was calculated as $CFU_{neutrophil\ or\ blood}/CFU_{medium\ or\ serum} \times 100\%$. Data in the graphs represent mean ± SEM of at least three independent experiments. *$p <$ 0.05, **$p <$ 0.01, ***$p <$ 0.001 (Wilcoxon signed rank test).

PMA stimulation, nearly all wild-type neutrophils lost their lobulated nuclear structures (Fig. 8B). Approximately half of the wild-type neutrophils formed either diffused or fully spread NET structures, and the remaining half of the neutrophils exhibited delobulated nuclei. In contrast, nearly half of the PMA-stimulated Gsr-deficient neutrophils retained their classic lobulated nuclear structures, whereas ~40% of these neutrophils displayed delobulated nuclear structures. Only a very small fraction (<10%) of Gsr-deficient neutrophils formed net-like structures (Fig. 8B).

Because NETs have been shown to contain histones and neutrophil antimicrobial proteins, we examined the cellular localization of these proteins. Immunofluorescence indicated that neutrophil elastase and histone H2A.X were retained within the

unstimulated neutrophils (Fig. 8C, *first* and *second rows*). In response to PMA stimulation, considerable morphological changes took place in wild-type neutrophils (Fig. 8C, *third row*). In these neutrophils, elastase spread out with histone H2A.X. Although Gsr-deficient neutrophils were also activated after PMA stimulation, as indicated by the cell flattening and membrane extension (Fig. 9B), few changes were seen in their nuclear structures, indicated by DNA staining and elastase distribution patterns (Fig. 8C, *bottom row*).

To characterize the defect of Gsr-deficient neutrophils in NET formation, we examined NETs formed by wild-type and Gsr-deficient neutrophils by using scanning electron microscopy (Fig. 9). Striking distinct morphological differences were observed between wild-type and Gsr-deficient neutrophils after both PMA and *E. coli* stimulation (Fig. 9). Unstimulated neutrophils isolated from both wild-type and Gsr-null mice were morphologically similar, appearing round with membrane folds on their surfaces (Fig. 9A). With PMA stimulation, a substantial fraction of neutrophils from wild-type mice underwent marked structural changes characteristic of NET extrusion (Fig. 9B, *upper panels*), which was reported in human neutrophils stimulated with PMA (19). After PMA stimulation, the cell membranes of the wild-type neutrophils ruptured and their chromatins were released, forming densely intertwined fibrous networks decorated with globular nodules. In contrast, most Gsr-deficient neutrophils flattened and spread onto the surface, forming the "fried egg" morphology with the cell debris left at the edge (Fig. 9B, *lower panels*). Very few of the Gsr-deficient neutrophils formed the NET structures after PMA stimulation. Incubation with *E. coli* also stimulated NET formation by wild-type neutrophils (Fig. 9C, *upper panels*). *E. coli* captured by the fibrous chromatin network was clearly seen. Although fibrous strands projecting from *E. coli*-infected Gsr-deficient neutrophils were occasionally observed, they did not form the mesh-like NET structures (Fig. 9C, *lower panels*). Moreover, the numbers of strands projected by these neutrophils were far fewer than those projected by wild-type neutrophils.

## Discussion

Previously, it has been reported that neutrophils isolated from a single family with marginal GSR activity exhibited a significant defect in the oxidative burst ex vivo (26). However, the bactericidal activity of the neutrophils was only marginally affected (26, 27). Because genetic differences between that family and other healthy controls were confounding factors, the significance of those studies awaited verification in better defined systems. In the present studies, we addressed the role of Gsr in host defense against bacterial challenge in vivo using a Gsr-deficient mouse model. By backcrossing Gsr-deficient mice to inbred C3H/HeN mice for 10 generations, we created Gsr-null mice on a pure genetic background. With this system, we eliminated the confounding factor of individual differences in genetic background associated with all human studies and overcame the ethical limitations in experimental methodology with human research subjects. In the present studies, we confirmed the findings made with GSR-deficient human neutrophils on the phagocytic defect in the oxidative burst (Figs. 6, 7). We further extended this line of investigation into an animal model of bacterial sepsis, and demonstrated that Gsr functions in vivo as an essential mediator in host defense against massive bacterial challenge (Figs. 1, 2). The following findings strongly suggest that intrinsic antimicrobial defects in phagocytes are responsible for the bactericidal defects found in Gsr-deficient mice. First, compared with wild-type mice there was no appreciable difference in either blood or bone marrow leukocyte composition in unstimulated Gsr-deficient mice. Second, *E. coli*-
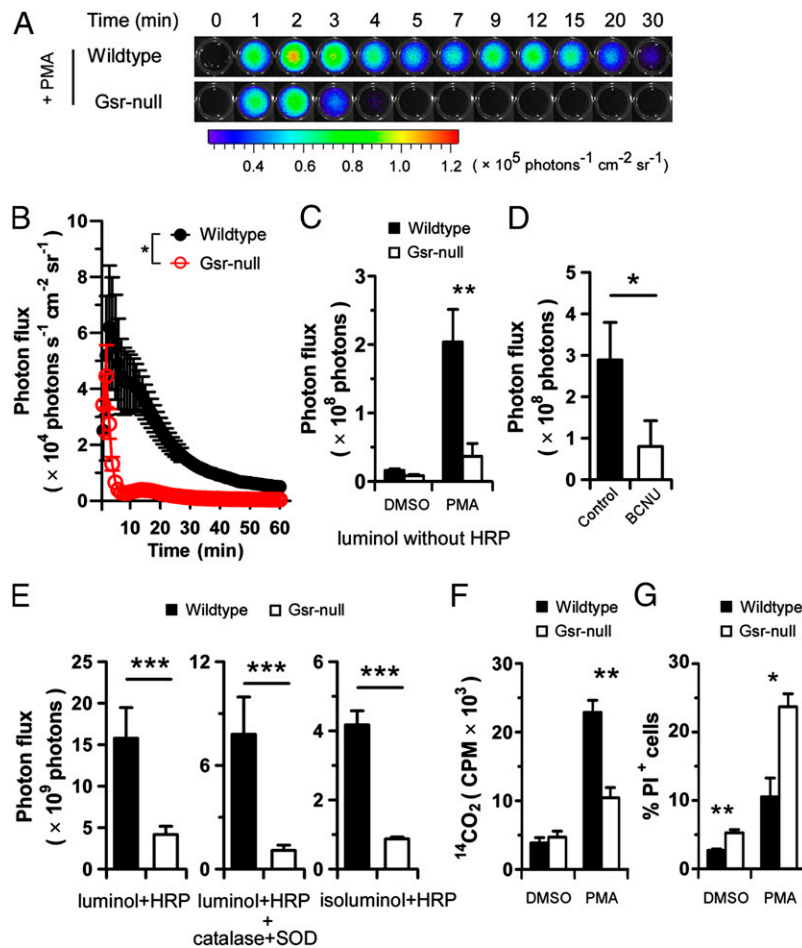
**FIGURE 6.** Gsr deficiency results in compromised phagocytic oxidative burst ex vivo following PMA stimulation. (**A**) Dynamic luminol chemiluminescence of PMA-stimulated blood leukocytes. Wild-type and Gsr-deficient mice were euthanized and blood was harvested by cardiac puncture. Blood cells were pelleted from 200 μl blood by centrifugation, and RBCs were lysed. The leukocytes were used to assess the oxidative burst following PMA stimulation in black 96-well plates, using luminol chemiluminescence in a Xenogen IVIS Spectrum imaging system. At $t = 0$, PMA (5 μM) was added. Bioluminescence was monitored by taking sequential images (exposure time, 1 min; field of vision, C; binning, 8) for 1 h. Photon influx images at indicated time points are shown. (**B**) Kinetics of oxidative burst in PMA-stimulated blood leukocytes ex vivo during 60 min. Photon influx in the wells at different time points were quantified and plotted against time in the graph. $*p < 0.05$, comparing the two groups over time (two-way ANOVA) ($n = 3$). (**C**) Total ROS production in blood leukocytes during 60 min. Total photon influx during 60 min was used as a surrogate for the accumulative ROS production. (**D**) Effect of BCNU on the PMA-induced oxidative burst in wild-type blood leukocytes. Wild-type blood leukocytes were treated with BCNU (1 μM) for 30 min and then stimulated with 5 μM PMA for assaying the oxidative burst. (**E**) Comparison of total, intracellular, and extracellular ROS production between wild-type and Gsr-deficient blood leukocytes. The oxidative burst was assessed by luminol chemiluminescence in the presence of HRP (representing total ROS produced, *left graph*) or HRP plus SOD and catalase (representing intracellular ROS produced, *middle graph*). Extracellular ROS was assessed using isoluminol in the presence of HRP. (**F**) HMPS activity in wild-type and Gsr-deficient neutrophils. Neutrophils were purified from bone marrow by Percoll gradient centrifugation. The neutrophils were stimulated either with vehicle (DMSO) or with PMA for 2 h in the presence of D-glucose-1-$^{14}$C. HMPS activity in the neutrophils was measured by assessing $^{14}CO_2$ production. Radioactivity in the captured $^{14}CO_2$ was measured in a scintillation counter. (**G**) The effect of PMA on neutrophil viability. Bone marrow neutrophils were stimulated with PMA (5 μM) or vehicle (DMSO) for 60 min. The viability of the cells was assessed by flow cytometry after incubated with PI. The portion of nonviable cells was expressed as percentage of PI$^+$ cells. Results shown in (A) are representative images. Values in bar graphs in (C)–(G) represent mean ± SEM from at least three independent experiments. $*p < 0.05$, $**p < 0.01$, $***p < 0.001$, comparing the two similarly treated groups (Wilcoxon signed rank test).

infected Gsr-deficient mice also had a blood leukocyte composition similar to that of infected wild-type mice (Table I), indicating normal leukocyte egress from the bone marrow postinfection. Third, Gsr-deficient phagocytes, particularly neutrophils, are defective in both phagocytosis (Fig. 5) and oxidative burst functions (Figs. 6, 7). Finally, neutrophils in Gsr-null mice exhibit a marked impairment in the development of NETs (Figs. 8, 9). Because of defects in these key bactericidal functions, it is not surprising that Gsr-deficient mice exhibited increased susceptibility to bacteria (Figs. 1A, 2, Table II).

The hepatic necrotic foci (Fig. 3A), the dramatic mortality and bacterial burdens (Figs. 1, 2), and the overwhelming cytokine storm after bacterial infection (Fig. 4) can be explained by the bactericidal defects of Gsr-deficient mice. The defective bacteri-

cidal activity may also explain the larger number of neutrophils seen in the red pulp region of the spleens of the Gsr-deficient mice than in those of the wild-type mice (Fig. 3B). The failure to clear the infecting *E. coli* in the Gsr-deficient mice may induce the production of chemokines, which in turn stimulate the egress of neutrophils from the bone marrow (47). The remarkable lymphocyte apoptosis in the white pulp of the spleens of *E. coli*-infected wild-type mice (Figs. 3B, 3C) may represent a resolution response after clearing the infection. Future studies are needed to understand the underlying mechanisms.

*The function of Gsr in phagocytic oxidative burst*

Gsr catalyzes the reduction of glutathione disulfide to glutathione, a major cellular antioxidant. Paradoxically, Gsr-deficient neu-
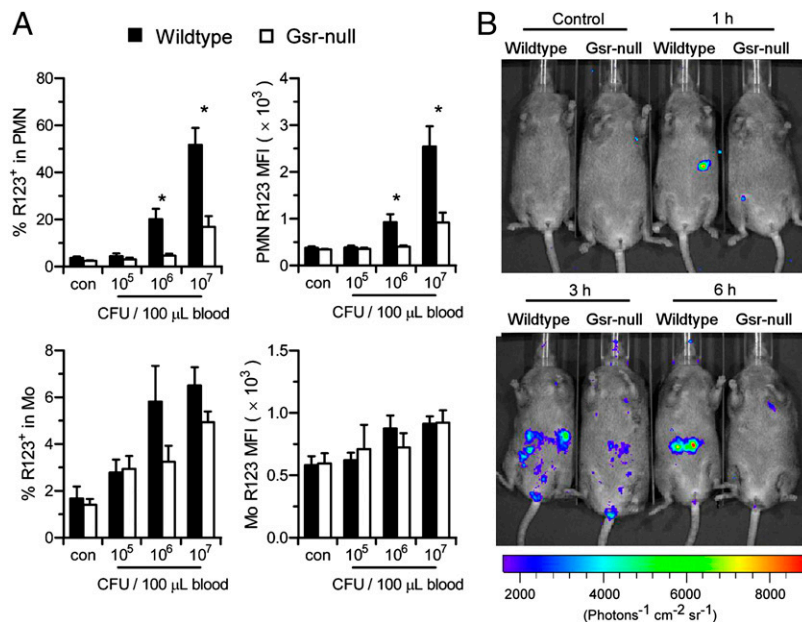
**FIGURE 7.** Gsr deficiency compromises the *E. coli*-induced phagocytic oxidative burst both ex vivo and in vivo. (**A**) ROS production measured by DHR123 oxidation in control and *E. coli*-stimulated blood neutrophils (PMN) and monocytes (Mo). Heparinized whole blood (100 μl) was incubated with indicated amounts of *E. coli* (O55:B5) in the presence of DHR123 for 15 min. The leukocytes were then stained with neutrophil and monocyte markers, and the oxidative burst activity in these cell populations was analyzed by flow cytometry. Percentages of neutrophils or monocytes that underwent oxidative burst (rhodamine 123+ cells, *left column*) and the mean intensity of oxidative burst in these rhodamine 123+ cells (MFI, *right column*) are shown. Values in bar graphs represent mean ± SEM from at least three independent experiments. *$p < 0.05$ (Wilcoxon signed rank test). (**B**) The oxidative burst in vivo in *E. coli*-challenged wild-type and Gsr-deficient mice detected by luminol chemiluminescence. Uninfected (control) or *E. coli*-infected mice were administered luminol (200 μg/g b.w.) at different time points after *E. coli* challenge (O55:B5, $8.3 \times 10^6$ CFU/g b.w.) to collect luminescent images (exposure time, 5 min; field of view, D; binning, 8). Control animals were given luminol only; the remaining animals were infected i.p. with *E. coli* and given luminol at the indicated time points.

trophils are impaired in their oxidative burst and produce less ROS (Figs. 6, 7). Although the exact mechanisms involved remain unclear, we can offer some speculations. One might argue that deficiency of Gsr in the germ line of the mutant mice might trigger

a compensatory antioxidant response, augmenting the cellular oxidative defense mechanisms, which in turn would decrease the net production of ROS in the Gsr-deficient phagocytes. Although we cannot rule out this possibility, we think this postulate is less

**FIGURE 8.** PMA-stimulated Gsr-deficient neutrophils exhibit defects in NET formation. (**A**) Sytox Green staining of DNA of wild-type and Gsr-deficient neutrophils. Bone marrow neutrophils were seeded on uncoated glass coverslips and cultured in the absence (control) or presence of PMA (100 nM) for 16 h. These cells were then stained with Sytox Green to detect their DNA. Cells were examined under a confocal microscope. Images were Z-stack projections constructed using LSM ZEN software. (**B**) Quantification of NET formation in wild-type and Gsr-deficient neutrophils stimulated with PMA or unstimulated (control). Neutrophils stained with Sytox Green as in (A) were categorized according to their morphologies into four subsets (lobulated neutrophils, delobulated neutrophils, diffused NETS, and spread NETs). Percentage of each subset is shown in the graphs as mean ± SEM from at least three independent experiments. **$p < 0.01$, ***$p < 0.001$ (Wilcoxon signed rank test). (**C**) Immunofluorescence of NETs in control and PMA-treated wild-type and Gsr-deficient neutrophils. Neutrophils were treated as in (A) and were then subjected to immunofluorescence with Abs against neutrophil elastase (NE, green) and histone 2A.X (magenta). Finally, DNA was stained with Hoechst 33342 (blue) and the cells were examined with confocal microscopy. Three-dimensional immunofluorescence images were obtained using z-stack projections. Images shown are representative of at least three independent experiments. Scale bars, 10 μm.
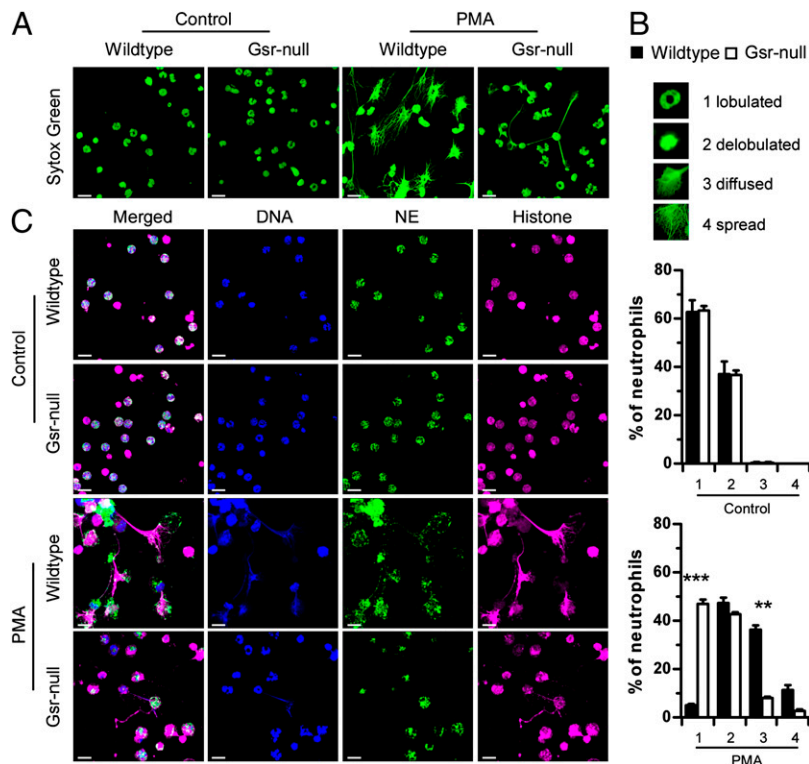
**FIGURE 9.** Gsr-deficient neutrophils fail to develop the characteristic NETs upon stimulation with PMA or *E. coli*. Bone marrow neutrophils were seeded on uncoated glass coverslips. These cells were stimulated for 16 h with DMSO (vehicle control) or PMA (100 nM) or with *E. coli* at a multiplicity of infection of 50 and subjected to scanning electron microscopy analysis. Images are representative of at least three independent experiments. Scale bars, 3 μm (lower magnification images), 0.6 μm (higher magnification images).
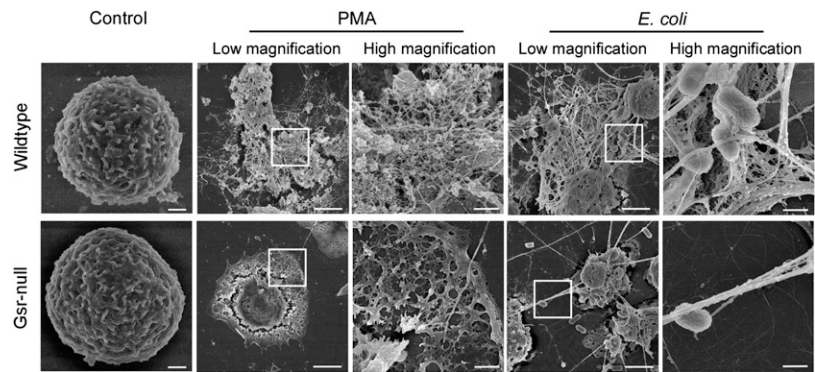
likely. First, the pharmacological inhibitor BCNU abolished the oxidative burst in wild-type cells (Fig. 6D). It is unlikely that a short pretreatment of wild-type phagocytes with BCNU would trigger a compensatory antioxidant response. Second, a stronger antioxidant compensatory mechanism cannot explain the decrease in HMPS activity in the Gsr-deficient neutrophils. Additionally, Roos et al. (27) have examined the activities of several key enzymes involved in oxidative metabolism, including glutathione peroxidase, catalase, SOD, and MPO in a family with GSR deficiency and found no differences in their activities from the normal control subjects. Perhaps the simplest explanation is that Gsr-deficient neutrophils are less resistant to the damaging effects of the oxidative burst (Fig. 6F). Although $H_2O_2$ and $O_2^{\bullet-}$ created through the oxidative burst are critical for the bactericidal activity in the phagolysosome, these ROS can cause oxidation and inactivation of a variety of the cell's own biomolecules when they leak into other compartments (48). Because NADPH oxidase complexes are assembled on the membrane of phagolysosomes, it is reasonable to speculate that $H_2O_2$ produced near the phagolysosome membrane diffuses not only into the phagolysosome, but also into the cytosol. In the cytosol, $H_2O_2$ is detoxified by glutathione, through a reaction mediated by glutathione peroxidase (23, 24). The cellular pool of glutathione is replenished by two mechanisms: glutathione regeneration from GSSG mediated by Gsr and de novo glutathione synthesis. By regenerating glutathione from GSSG, Gsr facilitates cytosolic $H_2O_2$ detoxification, which protects phagocytes from oxidative damage and sustains oxidative burst-mediated bactericidal activities (23, 24). Because Gsr-deficient neutrophils cannot regenerate glutathione, it is likely that once their glutathione is depleted, ROS will spill into the cytosol. Oxidation of biologically active molecules in the cytosol is likely to compromise neutrophil function and lead to cell death (48), a concept consistent with the lower viability of Gsr-deficient neutrophils following PMA treatment (Fig. 6G). This model predicts that Gsr becomes critically important only when glutathione is depleted in the cytosol, for example as a result of the high-intensity oxidative burst. Because the intensity of the oxidative burst in monocytes stimulated by *E. coli* is significantly lower than that in neutrophils (Fig. 7A), it is not surprising that we found that Gsr deficiency had little effect on the oxidative burst in monocytes (Fig. 7A).

An alternative postulate regarding the defective oxidative burst of Gsr-deficient neutrophils is that accumulation of GSSG in the Gsr-deficient neutrophils facilitates thiol–disulfide exchange reactions, leading to extensive protein *S*-glutathionylation in the cytosol. *S*-glutathionylation of thiol-containing proteins could inhibit a variety of biological functions (49), including the HMPS-coupled oxidative burst. Previously, protein *S*-glutathionylation has been observed in both neutrophils and macrophages during the

oxidative burst (50–53). Although characterization of the protein modifications in Gsr-deficient neutrophils may hold the key for the ultimate elucidation of the mechanisms underlying the bactericidal defects of Gsr-null mice, this will require extensive proteomic analyses and is beyond the scope of the current study. Regardless of whether proteins are oxidized and/or *S*-glutathionylated, such modifications are likely to have detrimental effects on the neutrophils, providing a plausible explanation for the lower viability of Gsr-deficient neutrophils than their wild-type counterparts after PMA stimulation (Fig. 6F). This is also consistent with the rapid cessation of the oxidative burst and the decreased HMPS activity in Gsr-deficient leukocytes after PMA stimulation (Fig. 6A, 6D).

Note that although Gsr-deficient mice exhibit a substantial decrease in the phagocytic oxidative burst activity, these mice still retain a significant portion of oxidative burst activity (~20% of wild-type mice) (Fig. 6). Previously it has been shown that CGD patients with modest residual ROS production have significantly less severe illness and greater likelihood of long-term survival than do patients with little residual ROS production (54). The significant portion of oxidative burst activity retained in the Gsr-deficient mice apparently is sufficient to prevent the development of CGD in these mice and explains why Gsr-deficient mice lack a discernable phenotype in the absence of massive bacterial challenge. This is also consistent with the lack of CGD in humans with marginal GSR activity (26, 27).

*The role of Gsr in phagocytosis*

Although the defect in the neutrophil oxidative burst in Gsr-deficient mice reported in this study mirrors the oxidative burst defect of the previously reported family deficient in GSR activity (26, 27), the Gsr deficiency in our mice and the GSR defect in the reported family had different effects on neutrophil phagocytic functions. Whereas murine neutrophils lacking Gsr protein exhibit a lower phagocytic activity (Fig. 5A), the human neutrophils from the family with a defective GSR did not exhibit any impairment in phagocytic activity (27). The exact cause of this discrepancy is unclear, but it is plausible that this discrepancy is due to different severities of the corresponding mutations. Although the nature of the genetic mutation in the reported GSR-deficient family is unknown, the GSR gene of that family likely retained partial function because residual GSR activity was detected in their leukocytes. In contrast, the Gsr-deficient mice reported in this study have a complete knockout of Gsr (29) and do not express any Gsr protein (data not shown). It is also possible that the discrepancy in phagocytic phenotypes between the reported GSR-deficient human and the Gsr-deficient mouse neutrophils may represent an evolutionary divergence in the biological processes regulating phagocytosis.

How does Gsr deficiency affect phagocytosis? Although the answer is unclear, there are several possible explanations. Depletion of glutathione stores in the neutrophils of the Gsr-deficient mice may contribute to their phagocytic defects. Phagocytosis is a highly dynamic process mediated by actin polymerization and depolymerization controlled by intricate signal transduction pathways (55, 56). It is conceivable that the engulfment of bacterial particles initiates the respiratory burst, and that the oxidation or *S*-glutathionylation of host proteins as a result of glutathione depletion or increased GSSG levels vastly changes the dynamics of the cellular events within the phagocytes, eventually compromising the phagocytic process. Additionally, rapid cessation of HMPS may switch off the energy supply necessary for phagocytosis (57). Furthermore, loss of viable phagocytes due to oxidative stress may also account for the compromised phagocytosis seen in the Gsr-null neutrophils.

*The role of Gsr in the development of NETs*

Perhaps the most exciting finding of this study is the impairment of Gsr-deficient neutrophils to form NETs in response to activation (Figs. 7, 8). Previously, it has been shown that NET formation in neutrophils depends on the oxidative burst (17), although it is unclear exactly how the oxidative burst mediates the development of NETs. On the one hand, it is not surprising that Gsr-deficient neutrophils exhibited defects in NET formation, since these cells failed to mount a persistent oxidative burst (Fig. 5). On the other hand, it is conceivable that Gsr-deficient neutrophils likely accumulate oxidants at an accelerated pace after activation, and yet they fail to develop NETs (Figs. 7, 8). These results suggest that accumulation of oxidants alone is not sufficient for NET formation in murine neutrophils. Alternatively, acute oxidant accumulation as a result of Gsr deficiency may lead to rapid neutrophil death, aborting the cellular program of NETosis and consequently abolishing NET-mediated antimicrobial activity. Although a few of the Gsr-deficient neutrophils were able to spread their DNA chromatin into the extracellular space, the strands were far fewer than what were seen with wild-type neutrophils, consistent with prematurely aborting NETosis (Fig. 8).

*GSR as targets for malaria and cancer drugs*

Human GSR protein is regarded as a potential drug target for the treatment of malaria and cancer (58–61). Because Gsr is essential for the innate immunity against bacterial challenge, there is a reasonable concern that drugs targeting human GSR may render people susceptible to bacterial infection. This is particularly relevant in developing countries where malaria is prevalent and bacterial infections are common, due to the lack of clean drinking water. Additionally, because cancer patients often have compromised immune systems, owing to exposure to chemotherapeutic drugs or radiation therapy, drugs inhibiting GSR may further weaken their immune systems and exacerbate the risk of bacterial infection.

In conclusion, we have identified an essential role of Gsr in the innate immune system against massive bacterial infection. Our findings illustrate an intricate relationship between bactericidal action and phagocyte protection. Moreover, our studies shed novel insights into the immunosuppressive mechanisms of oxidative stress and open new avenues for the prevention and treatment of bacterial infections. Our findings also raise concerns for the potential immunosuppressive side effect of GSR inhibitors as anti-malaria and anti-cancer drugs.

## Disclosures

K.P.F. is an employee of Caliper Life Sciences. An instrument and a bacterial strain made by Caliper Life Sciences were used in these studies. The remaining authors have no financial conflicts of interest.

## References

1. Klebanoff, S. J., and R. A. Clark. 1978. *The Neutrophil: Function and Clinical Disorders.* North-Holland Publishing, Amsterdam.
2. Balija, T. M., and S. F. Lowry. 2011. Lipopolysaccharide and sepsis-associated myocardial dysfunction. *Curr. Opin. Infect. Dis.* 24: 248–253.
3. Nathan, C. 2006. Neutrophils and immunity: challenges and opportunities. *Nat. Rev. Immunol.* 6: 173–182.
4. Lambeth, J. D. 2004. NOX enzymes and the biology of reactive oxygen. *Nat. Rev. Immunol.* 4: 181–189.
5. Babior, B. M. 2004. NADPH oxidase. *Curr. Opin. Immunol.* 16: 42–47.
6. Tardif, M., M. J. Rabiet, T. Christophe, M. D. Milcent, and F. Boulay. 1998. Isolation and characterization of a variant HL60 cell line defective in the activation of the NADPH oxidase by phorbol myristate acetate. *J. Immunol.* 161: 6885–6895.
7. Kennedy, A. D., and F. R. DeLeo. 2008. PI3K and NADPH oxidase: a class act. *Blood* 112: 4788–4789.
8. Ellson, C., K. Davidson, K. Anderson, L. R. Stephens, and P. T. Hawkins. 2006. PtdIns3P binding to the PX domain of p40$^{phox}$ is a physiological signal in NADPH oxidase activation. *EMBO J.* 25: 4468–4478.
9. Knaus, U. G., P. G. Heyworth, T. Evans, J. T. Curnutte, and G. M. Bokoch. 1991. Regulation of phagocyte oxygen radical production by the GTP-binding protein Rac 2. *Science* 254: 1512–1515.
10. Abo, A., E. Pick, A. Hall, N. Totty, C. G. Teahan, and A. W. Segal. 1991. Activation of the NADPH oxidase involves the small GTP-binding protein p21$^{rac1}$. *Nature* 353: 668–670.
11. Chen, J., H. Tang, N. Hay, J. Xu, and R. D. Ye. 2010. Akt isoforms differentially regulate neutrophil functions. *Blood* 115: 4237–4246.
12. Cheng, N., R. He, J. Tian, M. C. Dinauer, and R. D. Ye. 2007. A critical role of protein kinase Cδ activation loop phosphorylation in formyl-methionyl-leucyl-phenylalanine-induced phosphorylation of p47$^{phox}$ and rapid activation of nicotinamide adenine dinucleotide phosphate oxidase. *J. Immunol.* 179: 7720–7728.
13. Inanami, O., J. L. Johnson, J. K. McAdara, J. E. Benna, L. R. Faust, P. E. Newburger, and B. M. Babior. 1998. Activation of the leukocyte NADPH oxidase by phorbol ester requires the phosphorylation of p47$^{PHOX}$ on serine 303 or 304. *J. Biol. Chem.* 273: 9539–9543.
14. Hoyal, C. R., A. Gutierrez, B. M. Young, S. D. Catz, J. H. Lin, P. N. Tsichlis, and B. M. Babior. 2003. Modulation of p47$^{PHOX}$ activity by site-specific phosphorylation: Akt-dependent activation of the NADPH oxidase. *Proc. Natl. Acad. Sci. USA* 100: 5130–5135.
15. Heyworth, P. G., A. R. Cross, and J. T. Curnutte. 2003. Chronic granulomatous disease. *Curr. Opin. Immunol.* 15: 578–584.
16. Brinkmann, V., and A. Zychlinsky. 2007. Beneficial suicide: why neutrophils die to make NETs. *Nat. Rev. Microbiol.* 5: 577–582.
17. Fuchs, T. A., U. Abed, C. Goosmann, R. Hurwitz, I. Schulze, V. Wahn, Y. Weinrauch, V. Brinkmann, and A. Zychlinsky. 2007. Novel cell death program leads to neutrophil extracellular traps. *J. Cell Biol.* 176: 231–241.
18. Wartha, F., and B. Henriques-Normark. 2008. ETosis: a novel cell death pathway. *Sci. Signal.* 1: pe25.
19. Brinkmann, V., U. Reichard, C. Goosmann, B. Fauler, Y. Uhlemann, D. S. Weiss, Y. Weinrauch, and A. Zychlinsky. 2004. Neutrophil extracellular traps kill bacteria. *Science* 303: 1532–1535.
20. Pilsczek, F. H., D. Salina, K. K. Poon, C. Fahey, B. G. Yipp, C. D. Sibley, S. M. Robbins, F. H. Green, M. G. Surette, M. Sugai, et al. 2010. A novel mechanism of rapid nuclear neutrophil extracellular trap formation in response to *Staphylococcus aureus. J. Immunol.* 185: 7413–7425.
21. Bianchi, M., M. J. Niemiec, U. Siler, C. F. Urban, and J. Reichenbach. 2011. Restoration of anti-*Aspergillus* defense by neutrophil extracellular traps in human chronic granulomatous disease after gene therapy is calprotectin-dependent. *J. Allergy Clin. Immunol.* 127: 1243–1252, e7.
22. Lin, A. M., C. J. Rubin, R. Khandpur, J. Y. Wang, M. Riblett, S. Yalavarthi, E. C. Villanueva, P. Shah, M. J. Kaplan, and A. T. Bruce. 2011. Mast cells and neutrophils release IL-17 through extracellular trap formation in psoriasis. *J. Immunol.* 187: 490–500.
23. Reed, P. W. 1969. Glutathione and the hexose monophosphate shunt in phagocytizing and hydrogen peroxide-treated rat leukocytes. *J. Biol. Chem.* 244: 2459–2464.
24. Strauss, R. R., B. B. Paul, A. A. Jacobs, and A. J. Sbarra. 1969. The role of the phagocyte in host-parasite interactions. XIX. Leukocytic glutathione reductase and its involvement in phagocytosis. *Arch. Biochem. Biophys.* 135: 265–271.
25. Cohen, H. J., E. H. Tape, J. Novak, M. E. Chovaniec, P. Liegey, and J. C. Whitin. 1987. The role of glutathione reductase in maintaining human granulocyte function and sensitivity to exogenous H$_2$O$_2$. *Blood* 69: 493–500.
26. Loos, H., D. Roos, R. Weening, and J. Houwerzijl. 1976. Familial deficiency of glutathione reductase in human blood cells. *Blood* 48: 53–62.

27. Roos, D., R. S. Weening, A. A. Voetman, M. L. van Schaik, A. A. Bot, L. J. Meerhof, and J. A. Loos. 1979. Protection of phagocytic leukocytes by endogenous glutathione: studies in a family with glutathione reductase deficiency. *Blood* 53: 851–866.

28. Pretsch, W. 1999. Glutathione reductase activity deficiency in homozygous *Gr1*^aIN eu mice does not cause haemolytic anaemia. *Genet. Res.* 73: 1–5.

29. Rogers, L. K., T. Tamura, B. J. Rogers, S. E. Welty, T. N. Hansen, and C. V. Smith. 2004. Analyses of glutathione reductase hypomorphic mice indicate a genetic knockout. *Toxicol. Sci.* 82: 367–373.

30. Zhao, Q., X. Wang, L. D. Nelin, Y. Yao, R. Matta, M. E. Manson, R. S. Baliga, X. Meng, C. V. Smith, J. A. Bauer, et al. 2006. MAP kinase phosphatase 1 controls innate immune responses and suppresses endotoxic shock. *J. Exp. Med.* 203: 131–140.

31. Wang, X., X. Meng, J. R. Kuhlman, L. D. Nelin, K. K. Nicol, B. K. English, and Y. Liu. 2007. Knockout of Mkp-1 enhances the host inflammatory responses to Gram-positive bacteria. *J. Immunol.* 178: 5312–5320.

32. Frazier, W. J., X. Wang, L. M. Wancket, X. A. Li, X. Meng, L. D. Nelin, A. C. Cato, and Y. Liu. 2009. Increased inflammation, impaired bacterial clearance, and metabolic disruption after Gram-negative sepsis in *Mkp-1*-deficient mice. *J. Immunol.* 183: 7411–7419.

33. Georgel, P., K. Crozat, X. Lauth, E. Makrantonaki, H. Seltmann, S. Sovath, K. Hoebe, X. Du, S. Rutschmann, Z. Jiang, et al. 2005. A Toll-like receptor 2-responsive lipid effector pathway protects mammals against skin infections with Gram-positive bacteria. *Infect. Immun.* 73: 4512–4521.

34. Sharma, P. K., E. Engels, W. Van Oeveren, R. J. Ploeg, C. van Henny der Mei, H. J. Busscher, G. M. Van Dam, and G. Rakhorst. 2010. Spatiotemporal progression of localized bacterial peritonitis before and after open abdomen lavage monitored by in vivo bioluminescent imaging. *Surgery* 147: 89–97.

35. Boxio, R., C. Bossenmeyer-Pourié, N. Steinckwich, C. Dournon, and O. Nüsse. 2004. Mouse bone marrow contains large numbers of functionally competent neutrophils. *J. Leukoc. Biol.* 75: 604–611.

36. Gross, S., S. T. Gammon, B. L. Moss, D. Rauch, J. Harding, J. W. Heinecke, L. Ratner, and D. Piwnica-Worms. 2009. Bioluminescence imaging of myeloperoxidase activity in vivo. *Nat. Med.* 15: 455–461.

37. Kehrer, J. P. 1983. The effect of BCNU (carmustine) on tissue glutathione reductase activity. *Toxicol. Lett.* 17: 63–68.

38. Pachman, L. M., P. Jayanetra, and R. M. Rothberg. 1973. Rheumatoid sera and soluble complexes: nitroblue tetrazolium dye test and hexose monophosphate shunt activation. *Pediatrics* 52: 823–830.

39. Li, J., M. Gorospe, D. Hutter, J. Barnes, S. M. Keyse, and Y. Liu. 2001. Transcriptional induction of *MKP-1* in response to stress is associated with histone H3 phosphorylation-acetylation. *Mol. Cell. Biol.* 21: 8213–8224.

40. Chen, P., D. Hutter, X. Yang, M. Gorospe, R. J. Davis, and Y. Liu. 2001. Discordance between the binding affinity of mitogen-activated protein kinase subfamily members for MAP kinase phosphatase-2 and their ability to catalytically activate the phosphatase. *J. Biol. Chem.* 276: 29440–29449.

41. Edwards, J. L., J. Q. Shao, K. A. Ault, and M. A. Apicella. 2000. *Neisseria gonorrhoeae* elicits membrane ruffling and cytoskeletal rearrangements upon infection of primary human endocervical and ectocervical cells. *Infect. Immun.* 68: 5354–5363.

42. Chen, P., J. Li, J. Barnes, G. C. Kokkonen, J. C. Lee, and Y. Liu. 2002. Restraint of proinflammatory cytokine biosynthesis by mitogen-activated protein kinase phosphatase-1 in lipopolysaccharide-stimulated macrophages. *J. Immunol.* 169: 6408–6416.

43. Thrasher, A. J., N. H. Keep, F. Wientjes, and A. W. Segal. 1994. Chronic granulomatous disease. *Biochim. Biophys. Acta* 1227: 1–24.

44. Sriskandan, S., and D. M. Altmann. 2008. The immunology of sepsis. *J. Pathol.* 214: 211–223.

45. Klebanoff, S. J. 2005. Myeloperoxidase: friend and foe. *J. Leukoc. Biol.* 77: 598–625.

46. Takei, H., A. Araki, H. Watanabe, A. Ichinose, and F. Sendo. 1996. Rapid killing of human neutrophils by the potent activator phorbol 12-myristate 13-acetate (PMA) accompanied by changes different from typical apoptosis or necrosis. *J. Leukoc. Biol.* 59: 229–240.

47. Soehnlein, O., and L. Lindbom. 2010. Phagocyte partnership during the onset and resolution of inflammation. *Nat. Rev. Immunol.* 10: 427–439.

48. Koháryová, M., and M. Kolárová. 2008. Oxidative stress and thioredoxin system. *Gen. Physiol. Biophys.* 27: 71–84.

49. Dalle-Donne, I., R. Rossi, G. Colombo, D. Giustarini, and A. Milzani. 2009. Protein S-glutathionylation: a regulatory device from bacteria to humans. *Trends Biochem. Sci.* 34: 85–96.

50. Rokutan, K., J. A. Thomas, and R. B. Johnston, Jr. 1991. Phagocytosis and stimulation of the respiratory burst by phorbol diester initiate S-thiolation of specific proteins in macrophages. *J. Immunol.* 147: 260–264.

51. Seres, T., V. Ravichandran, T. Moriguchi, K. Rokutan, J. A. Thomas, and R. B. Johnston, Jr. 1996. Protein S-thiolation and dethiolation during the respiratory burst in human monocytes: a reversible post-translational modification with potential for buffering the effects of oxidant stress. *J. Immunol.* 156: 1973–1980.

52. Rinna, A., M. Torres, and H. J. Forman. 2006. Stimulation of the alveolar macrophage respiratory burst by ADP causes selective glutathionylation of protein tyrosine phosphatase 1B. *Free Radic. Biol. Med.* 41: 86–91.

53. Lim, S. Y., M. J. Raftery, J. Goyette, and C. L. Geczy. 2010. S-glutathionylation regulates inflammatory activities of S100A9. *J. Biol. Chem.* 285: 14377–14388.

54. Kuhns, D. B., W. G. Alvord, T. Heller, J. J. Feld, K. M. Pike, B. E. Marciano, G. Uzel, S. S. DeRavin, D. A. Priel, B. P. Soule, et al. 2010. Residual NADPH oxidase and survival in chronic granulomatous disease. *N. Engl. J. Med.* 363: 2600–2610.

55. Underhill, D. M., and A. Ozinsky. 2002. Phagocytosis of microbes: complexity in action. *Annu. Rev. Immunol.* 20: 825–852.

56. Greenberg, S., and S. Grinstein. 2002. Phagocytosis and innate immunity. *Curr. Opin. Immunol.* 14: 136–145.

57. Selvaraj, R. J., and A. J. Sbarra. 1966. Relationship of glycolytic and oxidative metabolism to particle entry and destruction in phagocytosing cells. *Nature* 211: 1272–1276.

58. Deponte, M., S. Urig, L. D. Arscott, K. Fritz-Wolf, R. Réau, C. Herold-Mende, S. Koncarevic, M. Meyer, E. Davioud-Charvet, D. P. Ballou, et al. 2005. Mechanistic studies on a novel, highly potent gold-phosphole inhibitor of human glutathione reductase. *J. Biol. Chem.* 280: 20628–20637.

59. Becker, K., C. Herold-Mende, J. J. Park, G. Lowe, and R. H. Schirmer. 2001. Human thioredoxin reductase is efficiently inhibited by (2,2':6',2''-terpyridine) platinum(II) complexes: possible implications for a novel antitumor strategy. *J. Med. Chem.* 44: 2784–2792.

60. Sarma, G. N., S. N. Savvides, K. Becker, M. Schirmer, R. H. Schirmer, and P. A. Karplus. 2003. Glutathione reductase of the malarial parasite *Plasmodium falciparum*: crystal structure and inhibitor development. *J. Mol. Biol.* 328: 893–907.

61. Davioud-Charvet, E., S. Delarue, C. Biot, B. Schwöbel, C. C. Boehme, A. Müssigbrodt, L. Maes, C. Sergheraert, P. Grellier, R. H. Schirmer, and K. Becker. 2001. A prodrug form of a *Plasmodium falciparum* glutathione reductase inhibitor conjugated with a 4-anilinoquinoline. *J. Med. Chem.* 44: 4268–4276.